Deep Mining 2012 — Y. Potvin (ed)

doi:10.36487/ACG_rep/1201_29_karampinos

Determination of rock mass failure and rock mass damage criteria for the felsic norites at Nickel Rim South Mine

E. Karampinos *Lassonde Institute of Mining, University of Toronto, Canada*

B. Simser *Xstrata Nickel Ltd., Canada*

J. Hadjigeorgiou *Lassonde Institute of Mining, University of Toronto, Canada*

Abstract

This paper presents a case study where in situ rock mass observations were complemented with 3D stress analysis modelling to establish a range of in situ failure criteria for the felsic norites at the Nickel Rim South Mine in Canada. The development and the degree of validation of site specific failure criteria have important implications in the design and support of excavations at depth. The case is made that the quality of these interpretations are limited by the quality of the available field data.

1 Introduction

The stability of excavations under high stress conditions is influenced by the behaviour of the surrounding rock mass. Consequently determining the in situ mechanical properties of jointed rock masses is of importance in identifying and predicting this behaviour. This, however, remains a major challenge in deep and high stress mines. Traditional approaches to accomplish this task often rely on the use of laboratory index tests and/or some type of rock mass classification scheme. Both approaches often use some form of data manipulation and extrapolation to derive what are described as “realistic failure criteria”. This paper presents a back analysis, in an underground hard rock mine, to identify the in situ failure criteria. In this investigation in situ observations were complemented with 3D stress analysis modelling to establish a range of in situ failure criteria for the felsic norites at the Nickel Rim South Mine in Canada.

The case study was selected based on the availability of relatively good quality data. The field data, collected during construction of Nickel Rim South Mine underground garage in good quality felsic norites, at a depth of 1,480 m, were complemented with field observations during construction. The garage was developed in three passes. The construction process was carefully monitored using the Sirovision system commercially available from CAE Mining. This allowed the development of 3D profiles of the rock mass at every construction stage. The recorded 3D images were then used to estimate the vertical and horizontal cracked zones induced in the rock mass. Furthermore, the recorded digital images were used to estimate the resulting broken ground zone in the rock mass. This was assumed as the difference between the design layout and the final survey layout.

The 3D boundary element stress analysis program Map3D (Wiles, 2011) was used to trace the resulting stress redistributions during the construction stages of the underground garage. This information was used in conjunction with field observations on the depth of stress induced fractures that resulted in broken and cracked zones, and the induced stresses at the transition of these zones. A major assumption in the undertaken analysis and interpretation is that a “broken zone” and a “cracked zone” correspond to a site specific failure criterion, Figure 1.

Following a series of trials and calibrations a site specific “rock mass damage criterion” was developed based on the observed limit of the outer cracked zone for the felsic norites. Similarly, a “rock mass failure criterion” was determined based on the calibration of the Map3D model to the inner broken ground zone.

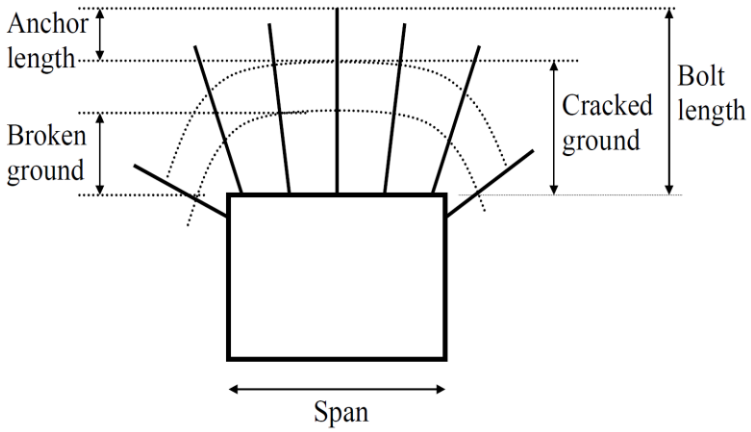

Figure 1 The stress induced broken and cracked zones, after Wiles et al. (2004)

The development of site specific failure criteria at the Nickel Rim South Mine has important implications in the design and support of excavations at depth. This investigation, however, raised some important questions on the obtained and acceptable degree of precision when moving from conceptual to in situ implementation of this type of analysis.

2 Nickel Rim South Mine

The Nickel Rim South Mine is located at the northeast side of the Sudbury Basin (Figure 2) in Canada and is owned by Xstrata Nickel. The deposit was discovered in 2001 and the mine was in full production in 2010 reaching over 1 Mt of ore per year (name plate design is 1.25 Mt/yr which was achieved in 2011).

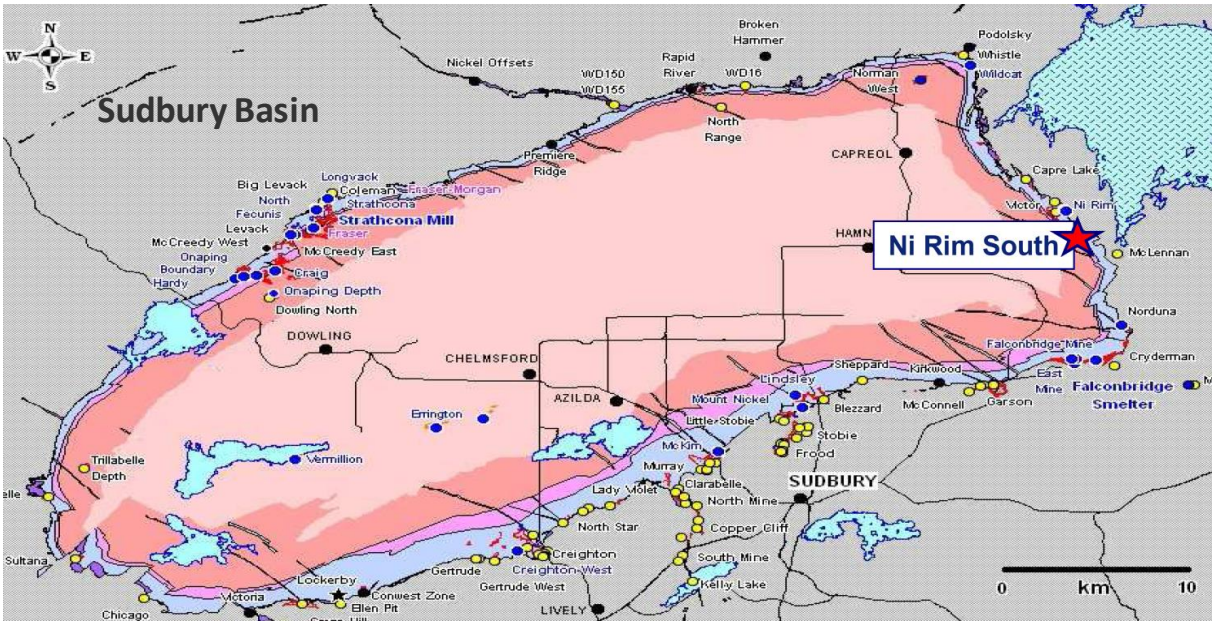

Figure 2 The location of Nickel Rim South Mine (Bartsch, 2009)

The mine comprises two geological zones, a hangingwall nickel sulphide orebody with average grades of 1.8% Ni and 1.2% Cu, and a footwall deposit of copper sulphide with 5.2% Cu, 1.5% Ni, 2.9 g/t Pt and 3.4 g/t Pd (Bartsch, 2009). Production goals are achieved from mining three main horizons: 1280 Nickel Zone; 1480 Copper Zone and Nickel Zones; and the 1660 Copper Zone. Access to these levels is possible through a 1,733 m deep shaft as shown in Figure 3. The mining method is transverse panel, primary/secondary open stoping with hydraulic tailings backfill.

The geology is relatively erratic and from a rock mechanics perspective it is important to note considerable variations in strength of the rock types found in the production areas. The host rock is what is often described as Sudbury breccia. In the copper zones of the mine, the unconfined compressive strength (UCS) of the intact rock is approximately 30 MPa for the copper sulphides, but can exceed 200 MPa in the host granitic breccia. Nickel zones in the mine display a lower variation between the host breccia (200 MPa) and the sulphides (115 MPa). The geomechanical model is further complicated by a number of faults and dykes traversing the orebodies (Simser and Pritchard, 2010).

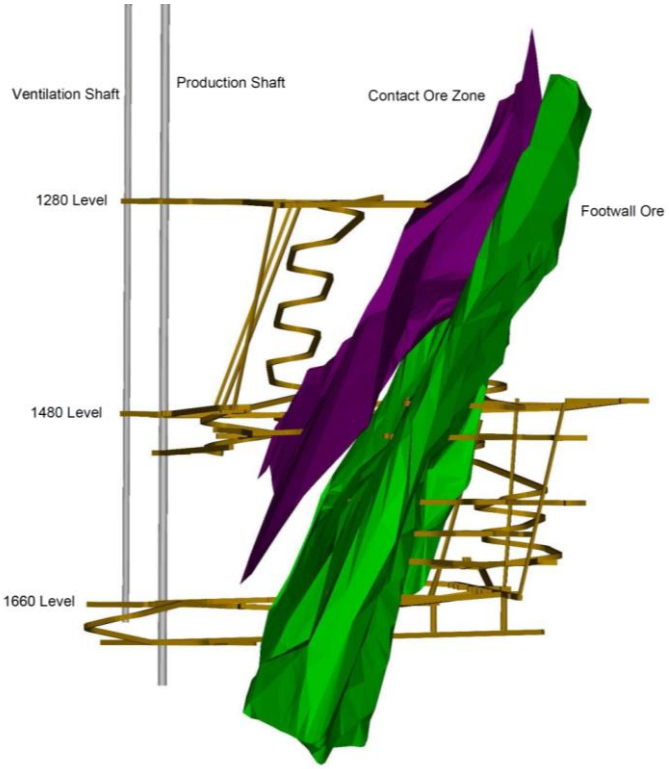

Figure 3 Schematic of Nickel Rim South Mine showing the ore zones, the three main horizons and the production and ventilation shaft (Bartsch, 2009)

3 Methodology

The construction of an underground garage in good quality felsic norites at Nickel Rim South Mine provided an opportunity to develop appropriate damage and failure criteria for the felsic norites. The underground garage was developed by drilling and blasting, in three stages, and with each advance step being 4 m long. The garage was constructed in what was perceived as good rock quality at a depth of 1,480 m, subjecting it to high stress conditions, Figure 4. The first stage resulted in a 10 m wide and 6.5 m high excavation which was widened to 16 × 6.5 m high. Subsequently, the height of the excavation was increased to 5 m resulting in the final garage dimensions of 16 m wide, 11.5 m high and 80 m long (Figure 4).

The construction process was monitored using the Sirovision system to develop 3D profiles of the rock mass during the widening and height increase of the first pass. The 3D images were used to estimate the cracked zones induced in the rock mass. Images taken during the development of the second pass indicated the depth of the vertical cracked zone induced during the first pass. Images taken during the third pass showed the depth of the horizontal cracked zone in the roof induced during the first and second pass. A broken ground zone was also defined as the difference between the design layout and the final survey layout.

A 3D boundary element program, Map3D Fault Slip (Wiles, 2011), was used to model the stress redistributions during the construction of the garage. A series of calibrations allowed the development of a

rock mass damage and a rock mass failure criterion based on the stress redistributions at the boundaries of the cracked zone and the broken zone respectively.

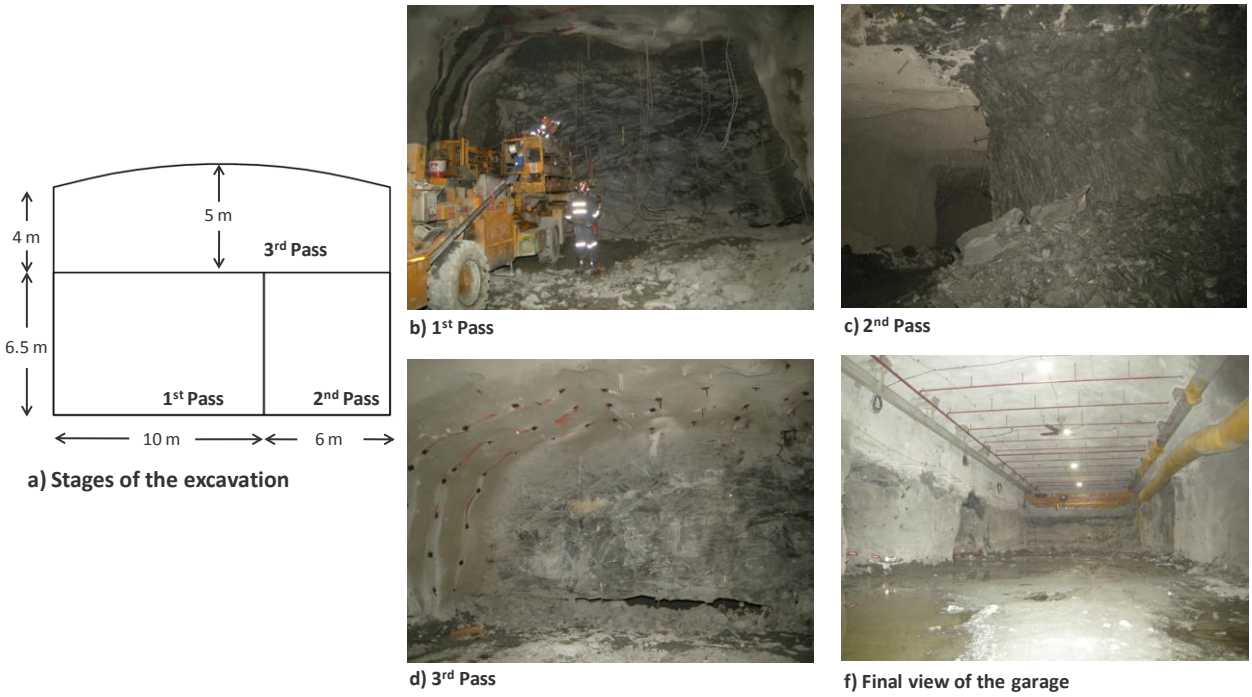

Figure 4 The three passes of the garage development and view of the garage after the completion of the 3rd pass

3.1 Rock mass characterisation

Pertinent geomechanical and rock mass damage information during construction was captured using Sirovision, a digital imaging system. A portable unit comprised by two cameras was used to capture a series of 2D images. The employed image analysis system uses photogrammetry principles and mathematical algorithms to extract 3D information from several 2D images. The generated output from matching several images is a virtual 3D copy of the mining excavation, Figure 5.

All images were recorded at a distance of approximately 6.5 m from the face and following high water pressure scaling of the walls and back and prior to installation of support. During this process photos were taken sequentially and ensuring a 1 m overlap which was adequate to reconstruct a 3D image. Once the 2D images were constructed in Sirovision software the mine introduced the 3D images in Datamine 3D studio, the geological modelling planning platform at Nickel Rim South.

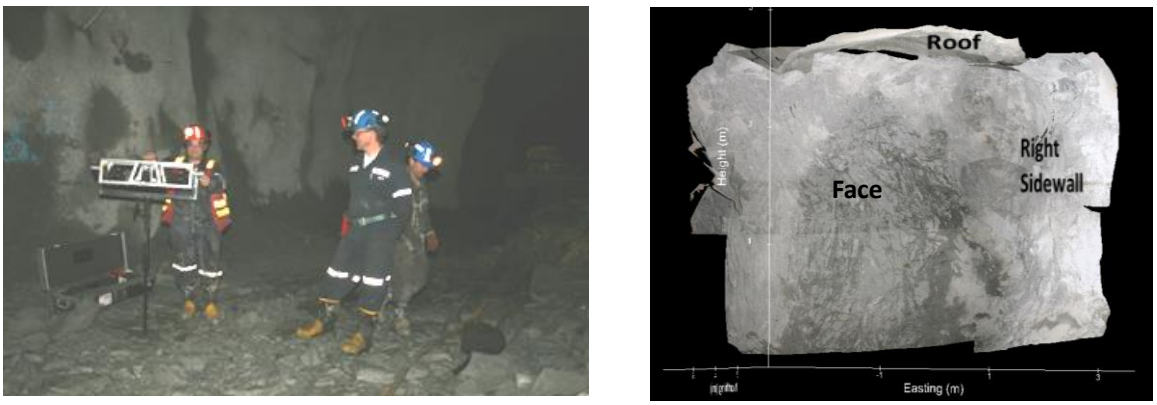

Figure 5 The Sirovision system equipment and a typical 3D image of the rock mass at Nickel Rim South Mine

3.2 Analysis of 3D images

The images were taken between December 2010 and May 2011, during the second and third pass in the development of the garage. The depth of the cracked zone was identified by the mine in July 2011. At the time it was observed that it was more difficult to identify the cracked zones in felsic norites compared with other more massive rock types mainly due to jointing interrupting the symmetry of the stress fracture pattern. Furthermore, it was difficult to establish a full reconciliation between the survey stations reference and the Sirovision images.

Blast induced fracturing was evident in all images. 3D images, taken during slashing of the excavation to 16 m wide (second pass) resulted to the most valuable data. Identifying the limits of the horizontal cracked zone from the 3D images taken during the third pass was more difficult. This was due to damage induced during the first two stages of excavation and the installation of cable bolts. Nevertheless, eight images taken during the second pass clearly indicated cracking induced during the first pass and ten images taken during the third pass showed the horizontal cracking induced during the first and second pass. The accuracy of the measurements was in decimetres which is well within the expectations for an operating mine. A typical image captured by Sirovision is reproduced in Figure 6(a) for the sidewall and in Figure 6(b) for the excavation back. Referring to the plan view diagrams, the location of the face, at the time when the image was captured is identified by the arrow. The average depth of fracturing observed for both vertical and horizontal stress is presented in Table 1. The depth of fractures corresponds to the distance of the highest upper boundary of the cracked ground.

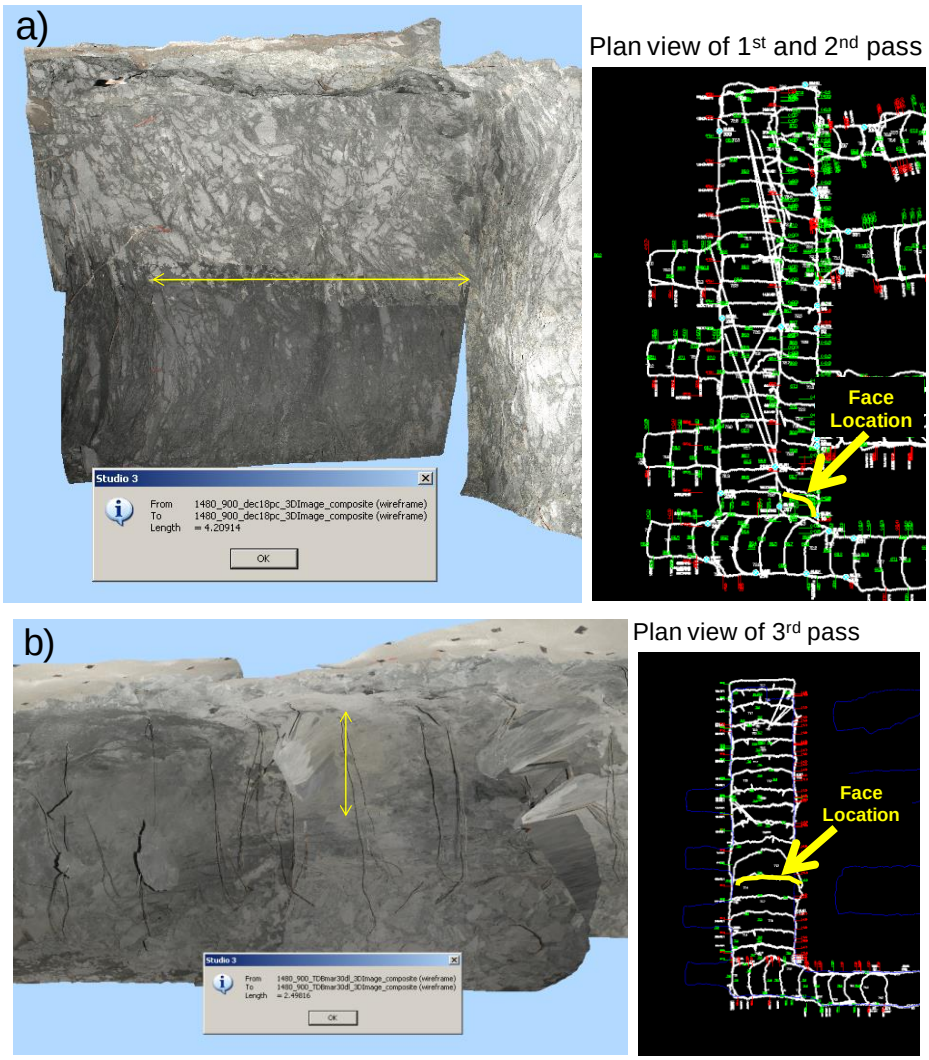

Figure 6 (a) Typical 3D image showing the vertical cracking in the sidewall; (b) Typical Sirovision image showing the horizontal cracking in the roof

Table 1 Depth of the fractures in the sidewall and the roof as to the design dimensions of the garage

Point Number	Depth of Fractures in the Sidewall Induced During 1st Pass (m)	Depth of Fractures in the Roof Induced During 1st and 2nd Pass (m)
1	2.1	2.7
2	2.2	0.8
3	1.1	1.9
4	2.1	1.8*
5	2.6	0.8
6	1.4	2.8
7	1.5	2.8
8	1.5	2.3
9	-	2.7
Average	1.81	2.08
Standard deviation	0.50	0.86

* Measurement shows the depth of the upper boundary of the cracked ground but disruptions on the Sirovision image did not allow identifying the higher upper boundary.

3.3 Numerical modelling

A 3D boundary element stress analysis software, Map3D Fault Slip (Wiles, 2011), was used to model each mining step and determine the identification of the stress redistribution during the excavation stages. An inherent assumption was that the rock mass in the vicinity of the underground garage behaved as a continuous, homogenous, isotropic and linear elastic medium. The mine has been using Map3D Fault Slip in order to aid with engineering decisions.

The interpretation of the analysis was based on the assumption that stress fracturing occurred immediately after blasting and prior to the installation of reinforcement and support. Typical seismic activity during the first hour following development blasts is presented in Figure 7 indicating that most of the seismicity occurs during that period and prior to the installation of support. This is illustrated in the diagram by stars for the development blasts and circles for the resulting seismic activity.

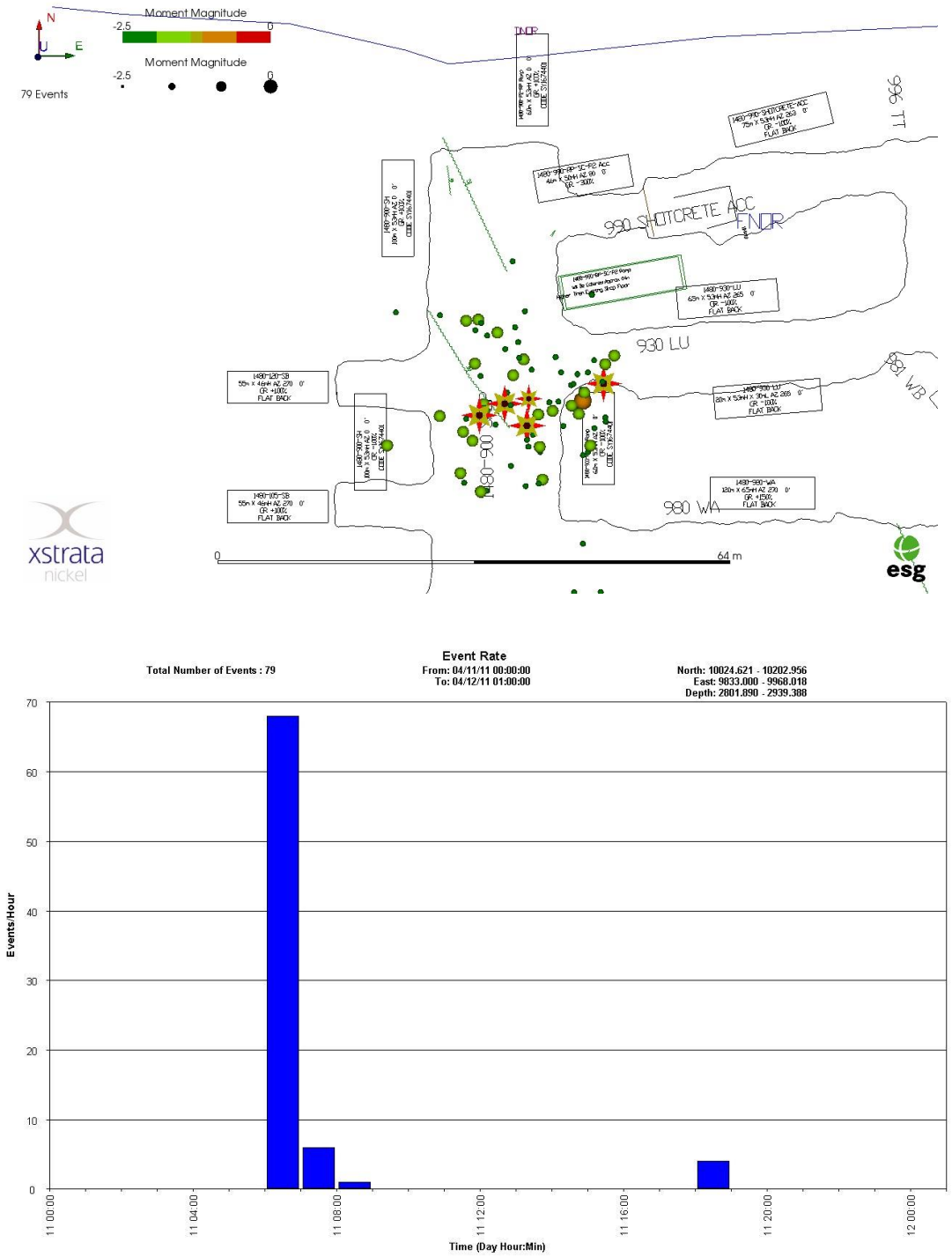

Figure 7 Typical seismic response detected during the first hour after development blast at the garage

Collecting quality stress data at deep mines is always a challenge. Nickel Rim South Mine has a series of stress measurements using the overcoring method which produced dubious results and one acoustic emission (AE) measurement. The AE measurement suggested that the principal stress (σ_1) is horizontal in the east–west direction, the minor horizontal stress (σ_2) has a north–south direction and σ_3 is the vertical stress. It was also determined that σ_1/σ_3 ratio was 1.6 and σ_2/σ_3 ratio was 1.2. This generally fits reasonably well with underground observations (depth of fracturing and hole breakouts) but anomalies are often noted, particularly near significant faulting.

The pre-mining stress conditions used at the model followed these values. The model considered one material (felsic norite) with Young's Modulus E = 33.5 GPa and Poisson's ratio v = 0.2. An average rock mass density of 0.026 MN/m^3 was chosen for the overburden. These values suggested that the pre-mining stresses at the garage area were: σ_1 = 61.5 MPa; σ_2 = 46.2 MPa; and σ_3 = 38.5 MPa. Different pre-mining stress conditions and mechanical properties were used during the calibration of the model and will be discussed below.

3.4 Construction of geometrical models

The construction of the geometrical models was based on the final survey layout of the garage area. For the developments around the garage, a 3D polyline representing the floor of the excavation was created in AutoCAD with the same x and y coordinates as the survey. A few floor height measurements (z coordinate) were available at the final survey. For that reason, the z coordinate chosen for each node during the polyline construction was the closest available. A 3D polyline was constructed for the roof using the same process. Blocks were created in Map3D by building every side surface separately. The blocks at the garage area were constructed following the design layout to allow the determination of the broken ground zone as the difference between the design and the final survey.

Figure 8 shows the model including the first pass and the developments around the garage. Mining steps during the construction stages are represented by different colours. At these locations 3D images indicated cracked zones.

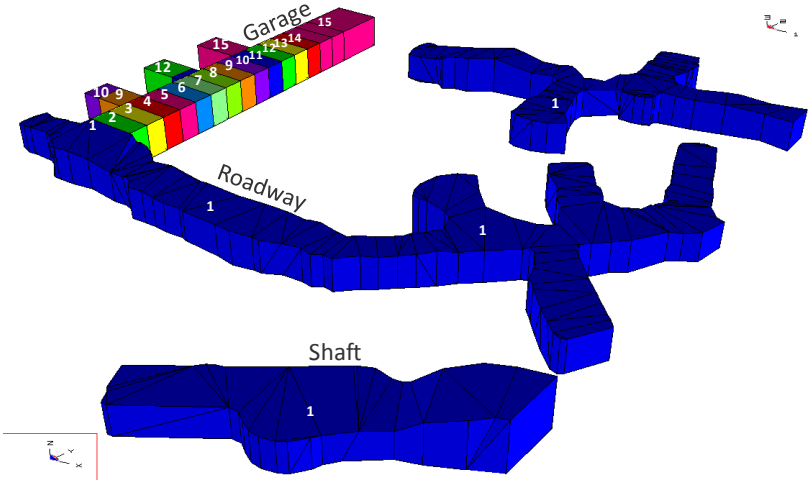

Figure 8 3D view of the Map3D model

3.5 Analysis

The followed procedure for the determination of the stress redistribution at the boundaries of the cracked zone is presented in Figure 9. A point at the upper boundary of the cracked zone was identified on each 3D image and its distance from the sidewall or roof was determined. The global coordinates of this point were then estimated from the survey. Subsequently, the stress redistributions at these points were identified within the stress analysis model.

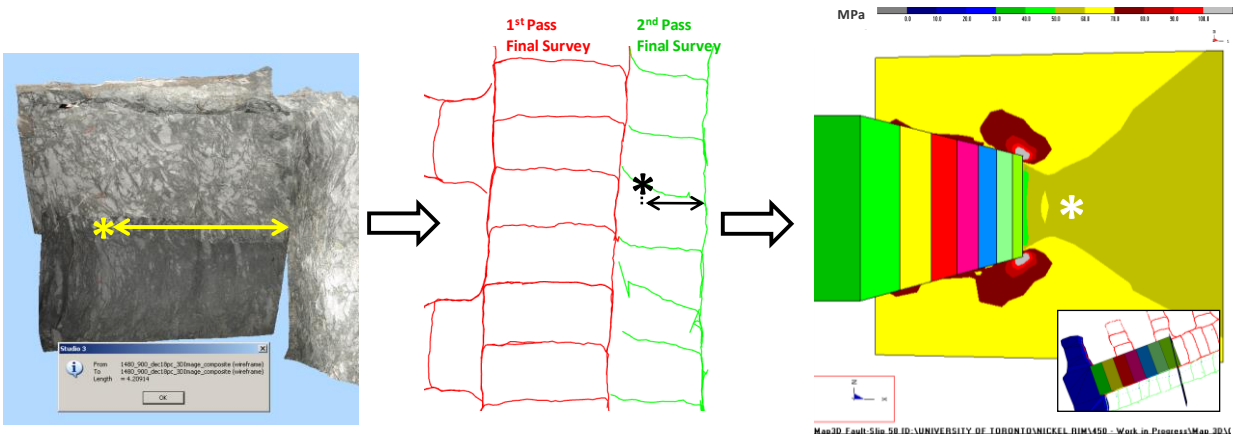

Figure 9 Procedure followed for the determination of the of the stress redistributions at the upper boundaries of the cracked zones

Figure 10 illustrates an example of the stress redistributions in the sidewall for the face position in December 18, 2010. The different steps used during the stress analysis resulted in the identification of σ_1 and σ_3 values at the upper boundaries of the cracked zone at the time and face position at which the cracking occurred.

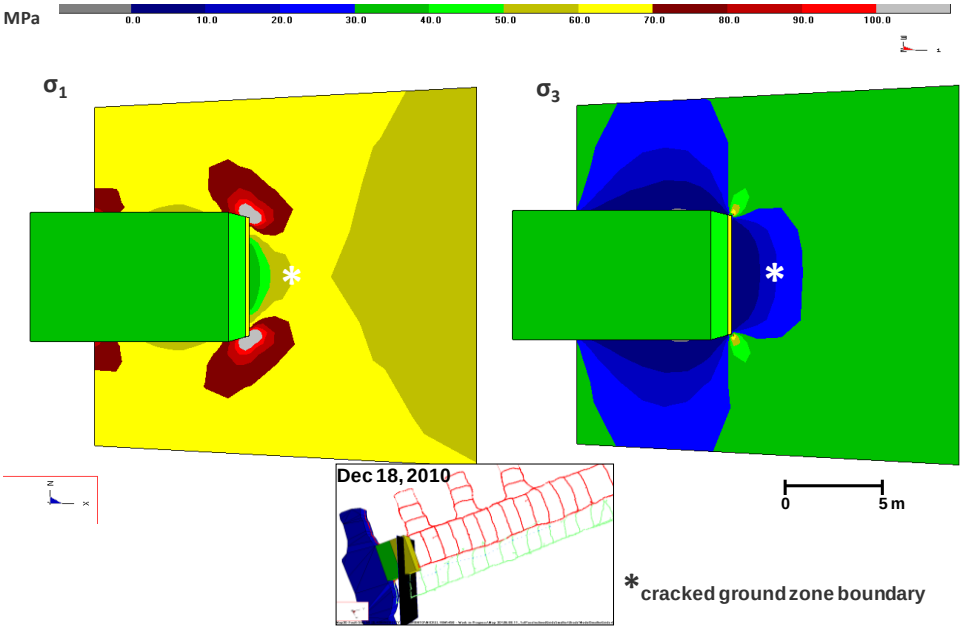

Figure 10 Typical stress redistributions in the sidewall during the first pass

A total of 463 points from the final survey were used to identify the broken ground zone. A small deviation between the design and the final survey layout was detected during the analysis as shown in Figure 11. This was due to overbreak.

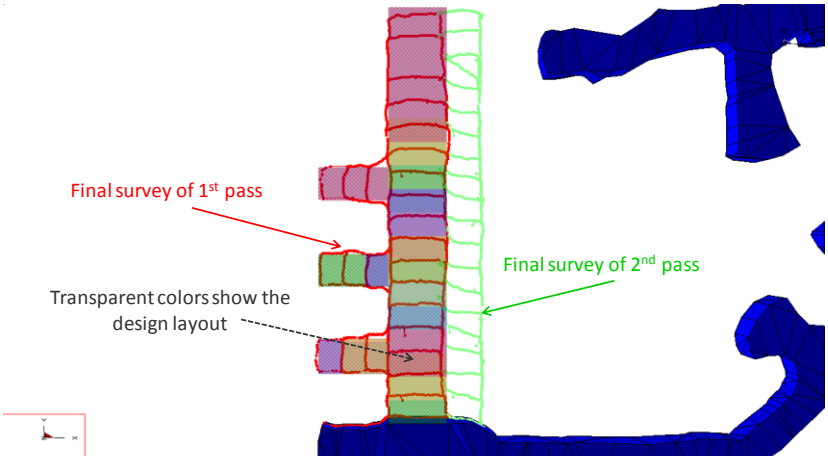

Figure 11 Deviation between the design and the final survey layout

4 Establishing rock mass strength criteria

Previous work by Wiles et al. (2004), and Louchnikov (2011) suggests that rock mass damage and rock mass failure criteria can be determined from back analysis assuming that the ground response can be described by broken ground and cracked ground zones as presented in Figure 12. Wiles et al. (2004) used the following criteria:

$$\sigma_1 = A + p\,\sigma_3 \text{ (rock mass damage criterion)} \quad (1)$$

$$\sigma_1 = B + q\,\sigma_3 \text{ (rock mass failure criterion)} \quad (2)$$

where A, B and p, q are site dependent constants, while Louchnikov (2011) used a strain failure criterion proposed by Stacey (1981).

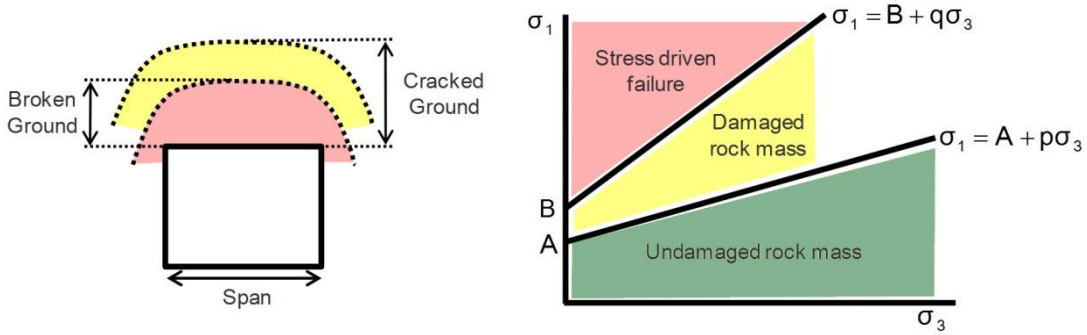

Figure 12 The stress induced broken and cracked zones, after Wiles et al. (2004)

4.1 Rock mass damage criterion

A rock mass damage criterion for the cracked ground zones at Nickel Rim South Mine is plotted in Figure 13. This was based on a calibrated model using a pre-mining stress K ratio (σ_1/σ_3) of 1.6. The principal horizontal stress at the boundaries of the cracked zone was approximately 20 MPa higher in the roof than the sidewall. This resulted in two trend lines and prompted further calibration efforts to obtain a rock mass damage criterion applicable to the sidewall and roof. A series of calibration tests were performed using different values for the pre-mining stress conditions and the mechanical properties. Changes in Young's Modulus and Poisson's ratio did not have significant effect on the rock mass damage criterion. However, it was observed that reducing the σ_1/σ_3 ratio, the deviation between the principal horizontal stress of the sidewall and the roof points was decreasing.

Figure 14 presents a single rock mass damage criterion for a σ_1/σ_3 ratio of 1.3. Assuming that the data is scattered around the best fit line following the normal distribution, the 5% and 95% probability contours are between $\Delta\sigma_1$ = ±9.7 MPa from the best fit line.

Figure 15 shows the $\Delta\sigma_1$ plot of the garage model for σ_1/σ_3 ratio of 1.3. It can be identified that for the same probability contours, the deepest the cracked zone can occur is 4.7 m and 12.6 m for the sidewall and the roof respectively.

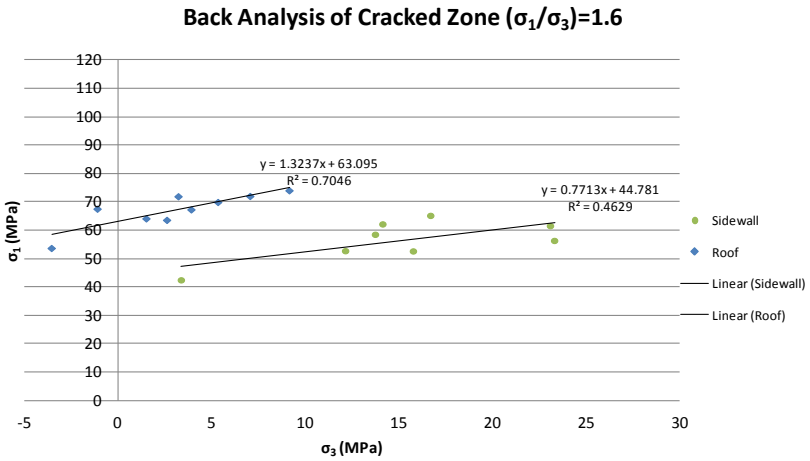

Figure 13 Back analysis of the cracked zones at felsic norite for σ_1/σ_3 of 1.6

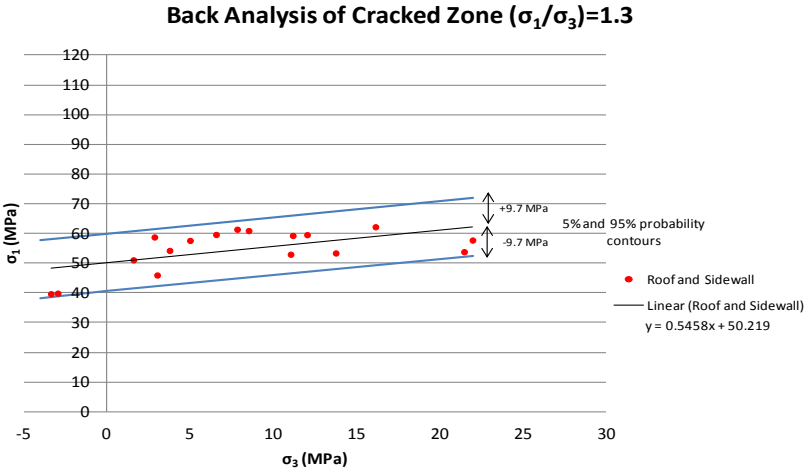

Figure 14 Back analysis of the cracked zones at felsic norite for σ_1/σ_3 of 1.3

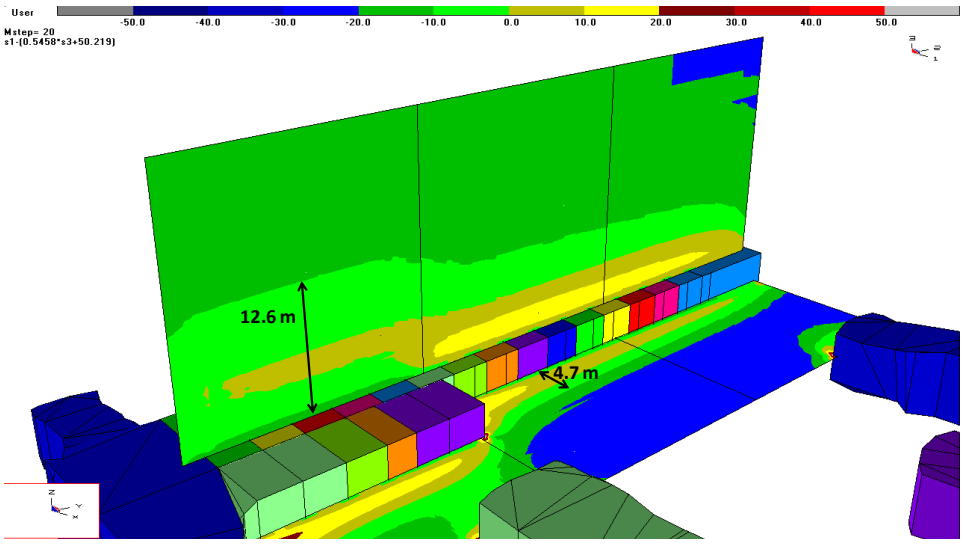

Figure 15 $\Delta\sigma_1$ plot for the garage model

The observed stress fracturing during the different phases of the garage excavation did imply the K ratio may locally be lower than 1.6, with relatively prominent vertical fracturing noted in the wall slash exposures. The garage area is relatively far from the mining zones at a distance of greater than 300 m, and has much less faulting, so it is plausible that a different K ratio may apply. The interpretation of the stress field is based on limited data and more work is required to verify possible variability.

4.2 Rock mass failure criterion

The magnitude of the principal horizontal stress and the vertical stress was identified at the boundaries of the broken ground zone to establish a rock mass failure criterion. Figures 16 and 17 illustrate the resulting σ_1/σ_3 values based on K ratios of 1.6 and 1.3 respectively.

The data is very scattered in both cases. It is believed that this is due to the deviation between the design and the actual layout. The zone of rock fall out is heavily influenced by blast damage and local jointing, so it is less likely to correlate as well with stress modelling results.

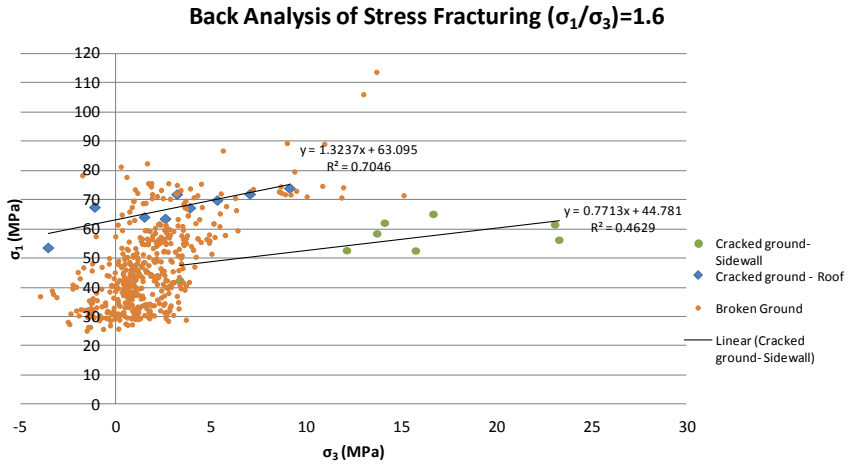

Figure 16 $\Delta\sigma_1$ plot for the garage model for σ_1/σ_3 of 1.6

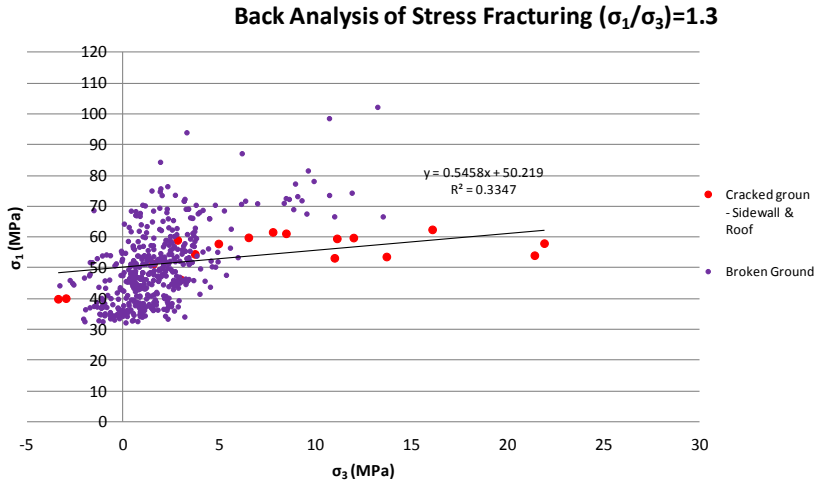

Figure 17 $\Delta\sigma_1$ plot for the garage model for σ_1/σ_3 of 1.3

5 Conclusions

This paper reports on the use of image analysis observations and numerical modelling to establish in situ failure criteria for the felsic norites at the Nickel Rim South Mine in Canada. The best fit failure criterion was based on a K ratio of 1.3, not the expected 1.6. It would appear that further work is required to better capture the in situ stress. As indicated in Figure 14, the trend obtained from stress analysis, correlated to the observed cracked zones from visual observations, was within ±9.7 MPa in the resulting σ_1 for the 5%

and 95% probability contours. These variations suggest that the interpretation of the stress model, with respect to the observed cracks has to be reassessed. In certain areas, near faults, there appears to be a degree of rotation as observed by the breakouts.

The undertaken work revealed the challenge in determining an acceptable precision in field data in an operating mine. It also reveals limitations in the homogenous rock mass assumption, some of the variations clearly came from the jointed nature of the rock mass which affects the observed fracture patterns around openings.

Based in the undertaken work there is a greater confidence in the developed rock mass damage criterion for the felsic norites than the rock mass failure criterion. Ongoing work aims to address the limitations of this analysis.

Acknowledgements

The authors would like to acknowledge the support of the Natural Science and Engineering Council of Canada. The field work was greatly facilitated by mine personnel at Nickel Rim South mine. Dr Terry Wiles of Mine Modelling PTY Limited provided some very useful suggestions.

References

Bartsch, E. (03/06/2009) Mine Wide SCADA System, Nickel Rim South Mine, Rockwell Automation Seminar, viewed 28 October 2011, http://www.myxps.ca/EN/Presentations/Documents/xps_speech_0906031_scada.pdf.

Louchnikov, V. (2011) Simple calibration of the extension strain criterion for its use in numerical modelling, in Proceedings from the Fourth International Seminar on Strategic versus Tactical Approaches in Mining, Y. Potvin (ed), Perth Australia, 8–10 November 2011, pp. 85–96.

Simser, B. and Pritchard, C.J. (2010) Observational Ground Control at Xstrata's Nickel Rim South Mine, in Proceedings of Maintenance Engineering and Mine Operations Conference 2010, 24–27 October, Sudbury, Canadian Institute of Mining, Sudbury, Canada.

Stacey, T.R. (1981) A Simple Extension Strain Criterion for Fracture of Brittle Rock, International Journal of Rock Mechanics and Mining Science and Geomechanics Abstracts, Pergamon Press Ltd, Vol. 18, pp. 469–474.

Wiles, T.D. (2011) Map3D V.58, www.map3d.com.

Wiles, T.D., Villaescusa, E. and Windsor, C.R. (2004) Rock reinforcement design for overstressed rock using three dimensional numerical modelling, in Proceedings Fifth International Symposium on Ground Support, Ground Support in Mining and Underground Construction, E. Villaescusa and Y. Potvin (eds), 28–30 September 2004, Perth, Australia, Australian Centre for Geomechanics, Perth, pp. 483–489.